Regional Chemostratigraphy and Mechanical Stratigraphy of the Barnett Shale, Fort Worth Basin, Texas

Alvarez, John., Alsleben, Helge

School of Geology, Energy, and the Environment, Texas Christian University, Fort Worth, TX 76107

Abstract

Although multiple localized chemostratigraphic and strength studies have been completed on the organic-rich Barnett Shale in the Fort Worth basin (Montgomery et al., 2005; Pollastro et al., 2007; Jarvie et al., 2007; Rowe et al., 2008; Williams et al., 2016; Taylor, 2017; Alsleben, unpublished), basin-wide correlations have not been completed. Basin-wide correlation of chemostratigraphy and mechanical stratigraphy could enhance the understanding of regional variations in chemical composition and rock competence. Therefore, the proposed study is going to test multiple hypotheses to identify regional trends and correlations within the Barnett Shale, based on variations in the formations chemical makeup and rock strength. Using the data from a total of nine cored Barnett intervals, several correlative chemofacies can be identified across the basin and grouped into zones. These zones show strong relationships between %Ca, %Si, % Clay (K, Al, Ti), and unconfined compressive strength.

Introduction

- Attempt to establish basin wide correlation between chemostratigraphic and mechanical stratigraphy components within the Barnett Shale (Fig. 1).
- Fort Worth Basin was a marine foreland basin created during the convergence of Laurentia and Gondwana (Fig. 2).
- Energy dispersive x-ray fluorescence (ED-XRF) and unconfined compressive strength (UCS) data collected at 3 inch intervals on a well from Archer county (Fig. 3).
- Data collected will be correlated to 8 other wells with similar data (Fig. 3).

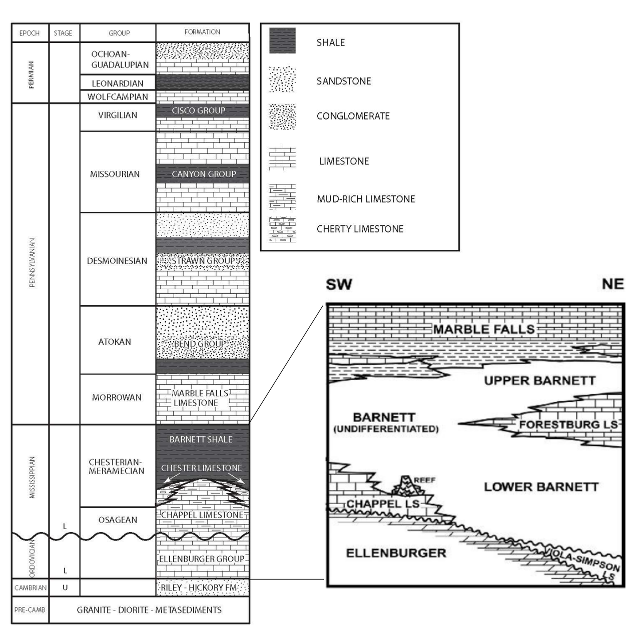

Figure 1. Stratigraphic column showing the general subsurface geology found in Fort Worth Basin

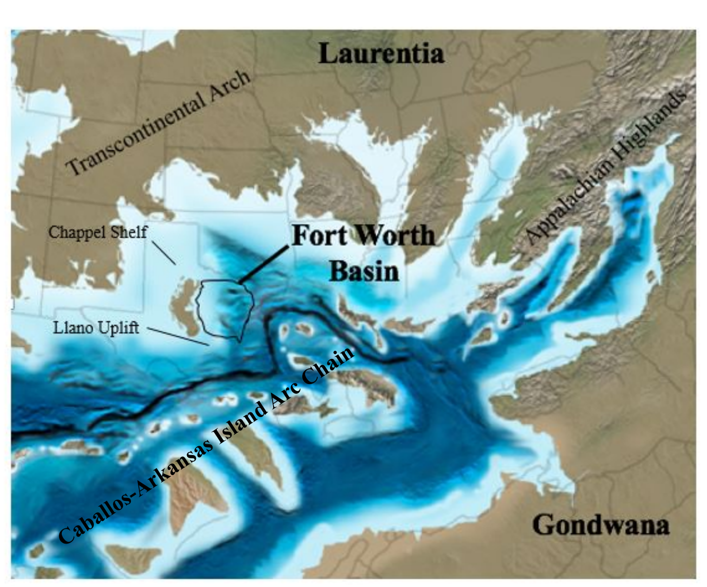

Figure 2. Regional paleogeography of the southern mid-continent region during he late Mississippian (325 Ma) showing the approximate location of the Fort Worth Basin outlined in black. (Modified from Blakey, 2005)

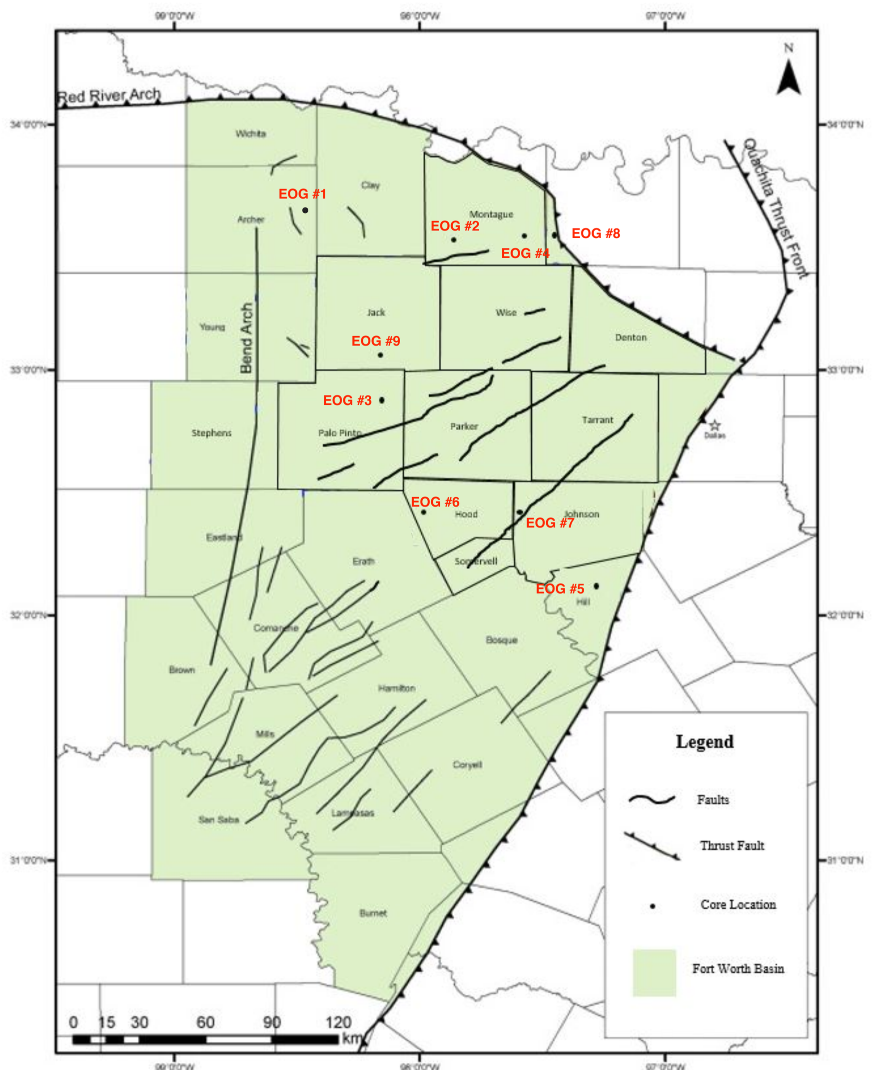

Figure 3. Map of Fort Worth Basin showing locations of faults, thrust front, and cores used in this study (Modified from Hornbach et al., 2016)

Methods

ED-XRF Analyses

- Elemental composition of samples were collected by Bruker Tracer IV (Fig. 4).
- ED-XRF can transmit and receive high-energy X-ray beams.
- Emitted X-ray force an electron to be expelled from the lower-energy inner shell (K shell), resulting in electrons from the higher-energy outer shells replacing the expelled electron and releasing energy in the form of emission X-rays (Fig. 5).
- Major element analysis will consist of a run time interval of sixty seconds with a 15kV calibration and trace element analysis will consist of a run time interval of ninety seconds with a 40kV calibration.
- Data is converted to weight% and parts per million (ppm).
- Heirarchical Cluster Analysis using the Ward (1963) method is performed on data from all nine cores to determine chemofacies.

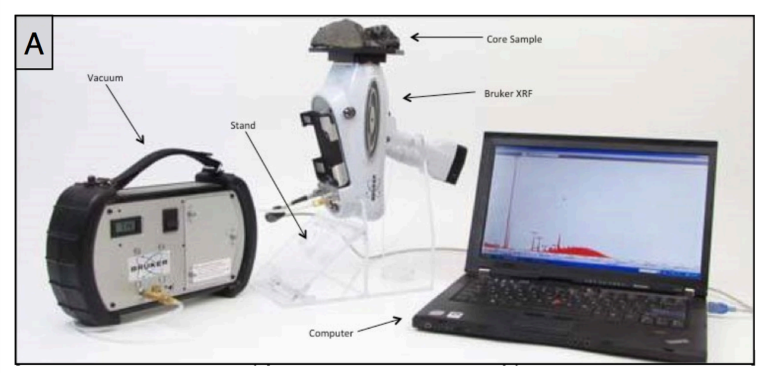

Figure 4. Image depicting the equipment used for ED-XRF analysis.

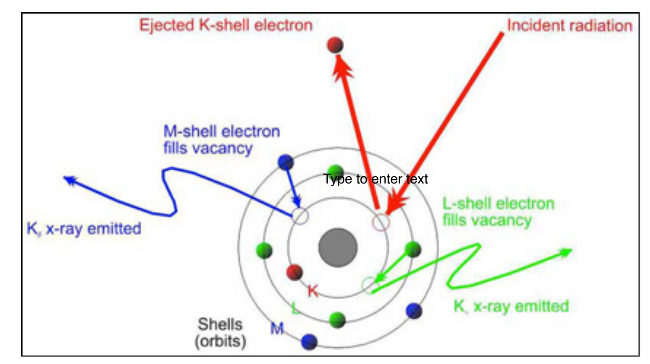

Figure 5. Generalized diagram showing how X-ray beams (incident radiation) from the XRF tool interact with electrons in an atom.

Micro-mechanical Analyses

- The Bambino (Fig.6) is a micro-rebound hammer used to measure Leeb's hardness number for each rock sample by measuring velocity at impact compared to rebound velocity (Fig. 7).
- An empirical equation from Zahm and Enderlin (2010) was used to convert Leeb Hardness into UCS.

Figure 6. Image of Equotip Bambino micro-rebound hammer.

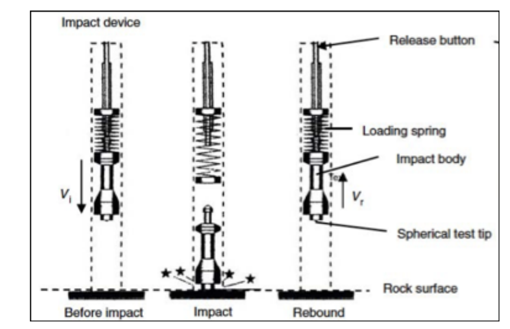

Figure 7. Schematic of Equotip Bambino. Modified from Aoki and Matsuura (2008)

- The Dimpler (Fig. 8) is a point-load penetrometer developed after Ramos et al. (2008).
- The impression (Fig. 9) left on the rocks surface can be measured and the geometric properties can be converted to UCS using an empirical equation from Ramos et al. (2008).

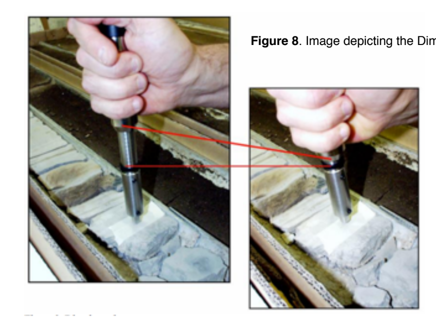

Figure 8. Image depicting the Dimpler tool in use.

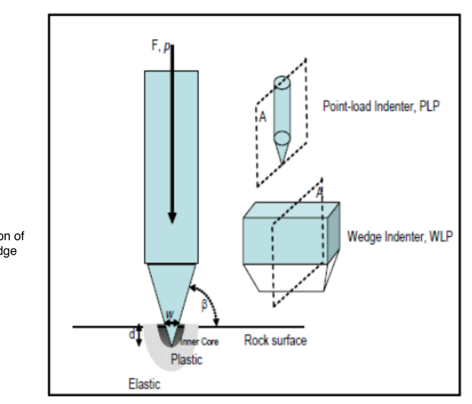

Figure 9. Illustration of point load and wedge shaped indenter

Results

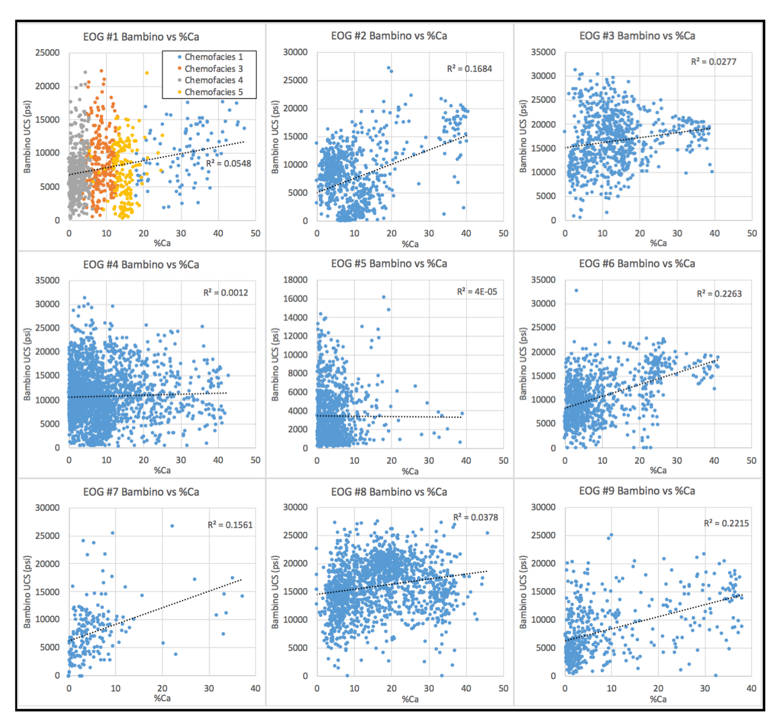

Figure 10. Crossplot of Equotip Bambino UCS vs %Ca in all nine wells.

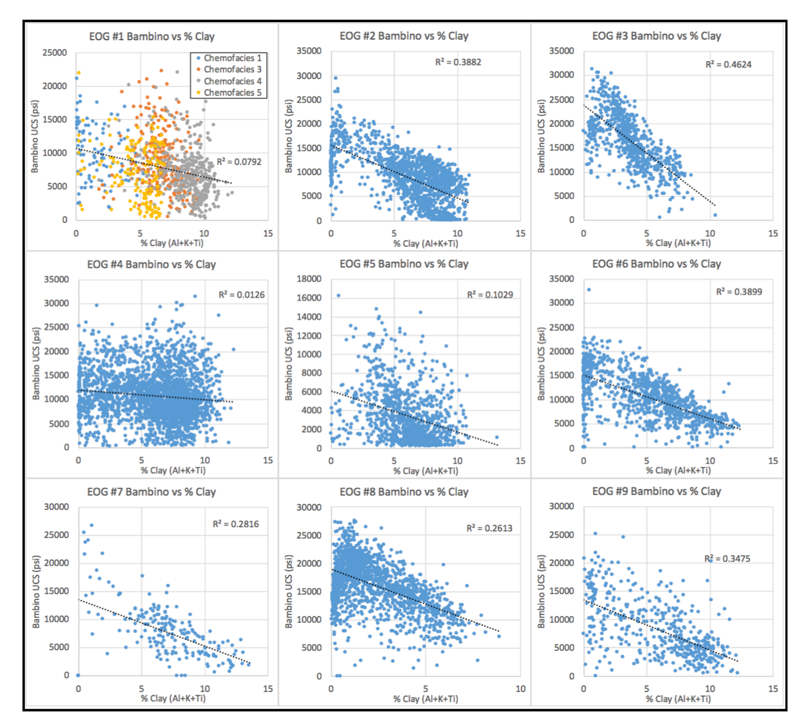

Figure 11. Crossplot of Equotip Bambino UCS vs %Clay (Al+Ti+K) in all nine wells.

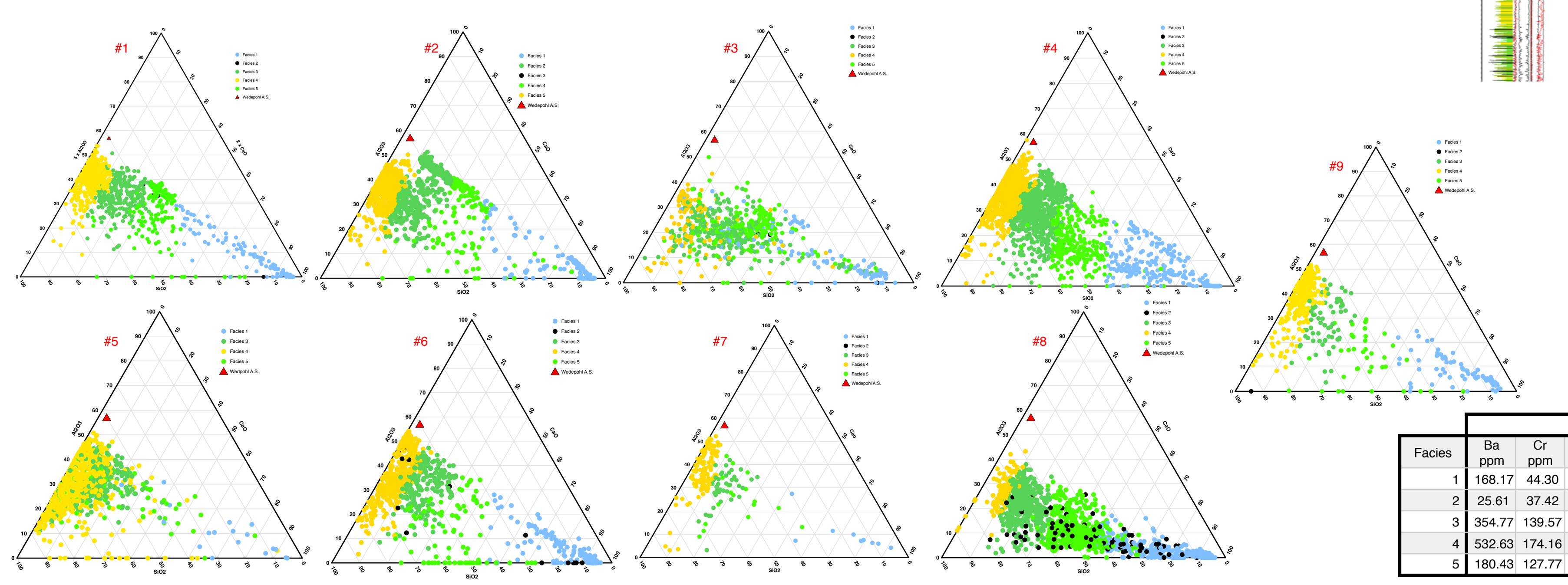

Figure 12. Ternary diagrams showing trends in minerals composition and chemofacies amongst all nine wells.

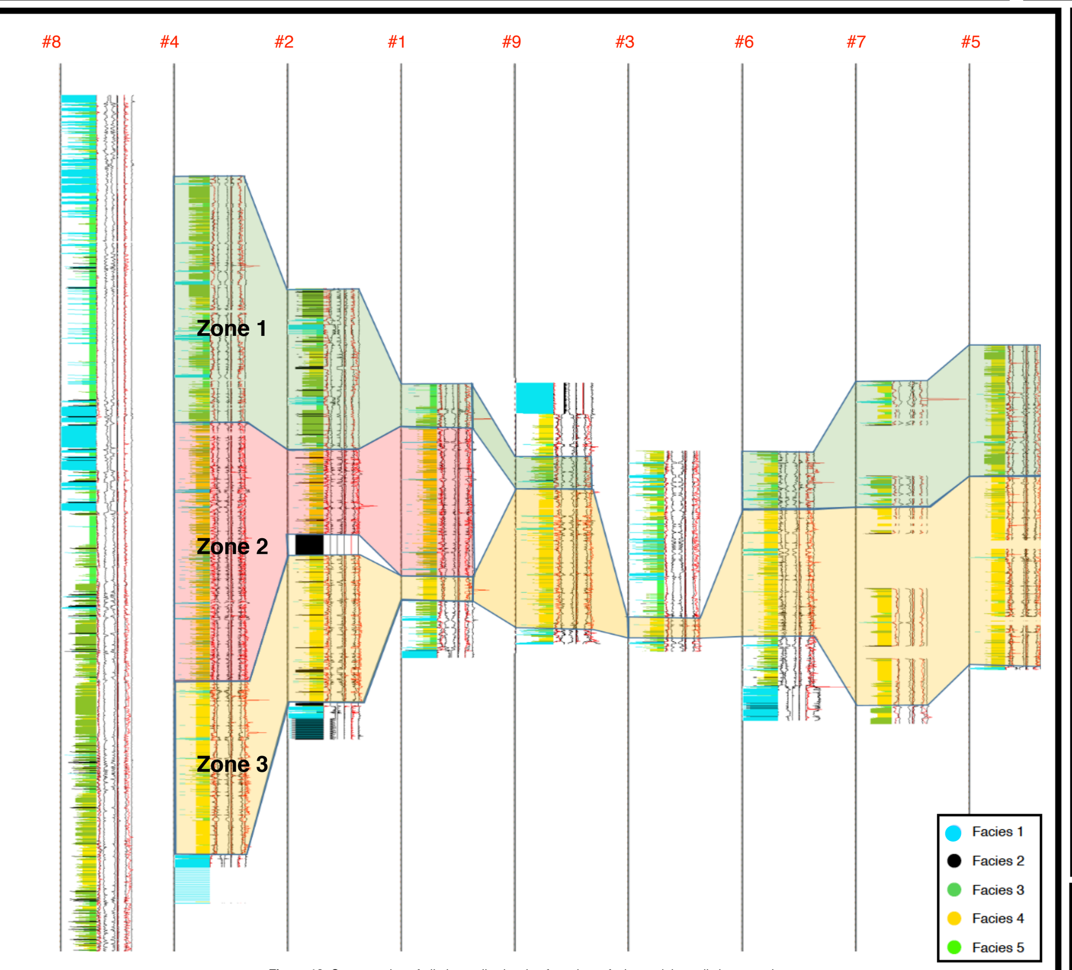

Figure 13. Cross-section of all nine wells showing four chemofacies and three distinct zonations. Wells are placed beside each other for easier correlation and are not plotted in relation to Total Vertical Depth (TVD).

	XRF Majors									
Facies	%Mg	%Al	%Si	%P	%S	%K	%Ca	%Ti	%Mn	%Fe
1	2.37	0.70	6.43	0.18	0.48	0.26	28.90	0.06	0.02	0.88
2	0.26	0.19	2.01	0.01	0.18	0.06	2.16	0.04	0.01	0.38
3	0.76	4.14	23.81	0.32	1.20	1.21	8.27	0.25	0.03	1.77
4	0.56	5.38	28.88	0.24	1.39	1.83	2.45	0.32	0.03	1.83
5	1.11	2.18	18.38	2.08	1.12	0.66	16.59	0.14	0.02	1.48

Figure 14. Table Showing the average %wt for each major element in relation to the chemofacies identified by a hierarchal cluster analysis.

	XRF Trace																	
Facies	Ba ppm	Cr ppm	Co ppm	Ni ppm	Cu ppm	Zn ppm	As ppm	Pb ppm	Th ppm	Rb ppm	U ppm	Sr ppm	Y ppm	Zr ppm	Nb ppm	Mo ppm	Sn ppm	Sb ppm	V ppm
1	168.17	44.30	5.29	37.42	8.43	55.08	18.18	8.48	3.09	18.98	5.38	719.79	19.27	26.14	4.00	4.62	1.75	5.32	59.40
2	25.61	37.42	1.95	20.72	14.30	35.14	1.72	2.45	0.97	7.21	2.29	247.70	6.00	6.29	1.40	1.46	0.15	0.40	0.49
3	354.77	139.57	10.44	77.61	34.30	184.36	9.98	9.50	5.71	70.20	8.09	632.38	31.78	71.16	7.12	18.69	2.12	6.49	97.65
4	532.63	174.16	11.54	100.47	48.81	261.35	13.07	9.36	6.68	94.83	5.66	309.23	30.96	89.60	6.82	28.88	2.36	7.76	124.02
5	180.43	127.77	8.27	58.90	22.30	128.22	8.53	9.35	4.40	44.52	11.77	919.58	34.23	42.66	7.02	10.67	1.64	5.38	64.77

Figure 14. Table Showing the average %wt for each trace element in relation to the chemofacies identified by a hierarchal cluster analysis.

Discussion

Results from strength and elemental testing show a strong positive linear relationship between %Ca and UCS (Fig. 10), as well as a strong negative linear relationship between %Clay (Al+Ti+K) and UCS (Fig. 11). Trends in minerals composition plot very closely between all nine wells and plot below the Wedepohl (1971) "Average Shale" (Fig. 12). Four distinct chemofaces were identified across all nine wells (Fig. 14)(Fig.15). Facies 2 is considered a quasi-facies as it is made up of the well sections were there was corrupt data or no data. Facies 1 and 5 are found mostly in the northern part of the basin and represent the most calcareous facies, suggesting sediment input from the Chappel Shelf. Facies 3 and 4 are found mostly in the southern part of the basin and represent the most silica and clay rich facies, suggesting sediment input from the Caballos-Arkansas Island Chain. Facies 4 trace elements (Mo, Ni,V, Cu, Zn, Co) suggest this facies was associated with the most authigenic enrichment under anoxic conditions (Tribovillard et al., 2006). Three zonations were identified by abundances of chemofacies in distinct sections of each well (Fig 13). Zone 1 being composed of mostly facies 3, zone 2 being composed of highly intertwined facies 3 and 4, and zone 3 composed of mostly Facies 4.

Conclusions

- In the Barnett Shale, clay content appears to have the largest effect on rock strength. The strongest rock being found in the northern part of the basin and the weakest rock being found in the southern part of the basin.
- 4 distinct chemofacies were identified across the basin using a hierarchical cluster analysis and then visually grouped into 3 unique zonations.
- Zonations suggest changes in sediment input in relation to location within the basin, with more calcareous input in the northern part of the basin, and more siliceous input in the southern part of the basin.

References

Blakey, R., 2005, Paleogeography and geologic evolution of North America; images that track the ancient landscapes of North America: http://jan.ucc.nau.edu/rcb7/nam.html. Accessed April 2017.

Burgess, W.J., 1976, Geologic evolution of mid-continent and Gulf Coast areas; plate tectonics view: Gulf Coast Association of Geological Societies Transactions, v. 26, p. 132-143.

Bruker. 2017. Tracer Series Overview. https://www.bruker.com/products/x-ray-diffraction-and-elemental-analysis/handheld-xrf/tracer-iii/overview.html. Accessed April 16, 2017.

Deere, D.U., and Miller, R.P., 1966, Engineering classification and index properties for intact rock; Univ. Illinois Contract AF29(601)-6319, Tech. Rept. AFWL-TR-65-116: United States (USA), p. 300.

Enderlin, M.B., 2010, A method for evaluating the effects of stresses and rock strength on fluid flow along the surfaces of mechanical discontinuities in low permeability rocks: [Master's thesis], Texas Christian University, Fort Worth, TX.

Fitton, G., 1997, X-ray fluorescence spectrometry, *in* Gill, R., ed., Modern Analytical Geochemistry: An Introduction to Quantitative Chemical Analysis for Earth, Environmental and Material Scientists: Essex, United Kingdom, Addison Wesley Longman, p. 87-115.

Henry, J.D., 1982, Stratigraphy of the Barnett Shale (Mississippian) and associated reefs in the northern Fort Worth basin, *in* Martin, C.A., ed., Petroleum geology of the Fort Worth basin and Bend arch area: Dallas Geological Society, p. 157-178.

Hoelke, J.D., 2011, Chemostratigraphy and paleoceanography of the Mississippian Barnett Formation, southern Fort Worth basin, Texas, USA:[Master's thesis], The University of Texas at Arlington, Arlington, Texas.

Hornbach, M.J., Jones, M., Scales, M., DeShon, H.R., Magnani, M.B., Frohlich, C., Stump, B., Hayward, C., and Layton, M., 2016, Ellenburger wastewater injection and seismicity in North Texas. Physics of the Earth and Planetary Interiors, v. 261, p. 54-68

Jarvie, D.M., Hill, R.J. Ruble, T.E., and Pollastro, R.M., 2007, Unconventional shale-gas systems: The Mississippian Barnett Shale of north-central Texas as one model for thermogenic shale-gas assessment: AAPG Bulletin, v. 91, p. 475-499.

Kiesel, M., 2013, Chemostratigraphy and Elemental Analysis of the Mississippian Barnett Shale Formation using Energy-dispersive X-ray Fluorescence Spectrometry, Fort Worth Basin, Johnson County, Texas: [Master's thesis], Texas Christian University, Fort Worth, TX.

Pollastro, R.M., Jarvie, D.M., Hill, R.J., and Adams, C.W., 2007, Geologic framework of the Mississippian Barnett-Paleozoic total petroleum system, Bend arch-Fort Worth Basin, Texas: AAPG Bulletin, v. 91, p. 405-436.

Rowe, H.C., Loucks, R.G., Ruppel, S.C., Rimmer, S.M., 2008. Mississippian Barnett Formation, Fort Worth Basin, Texas: Bulk geochemical inferences and Mo-TOC constraints on the severity of hydrographic restriction: Chemical Geology, v. 257 p. 16-25.

Taylor, C.Z., 2017, Chemostratigraphy, mechanical stratigraphy, and sample size influence on micro-mechanical tests for two Barnett shale cores, Fort Worth Basin, Texas: [Master's thesis], Texas Christian University, Fort Worth, TX.

Tribovillard, N., Algeo, T., Lyons, T.W. and Riboulleau, A. 2006. Trace metals as paleoredox and paleoproductivity proxies; an update 2006. Chemical Geology, v. 232, p. 12-32.

Williams, J.W., Alsleben, H., Enderlin, M.B., 2016, Correlation between rock strength and chemostratigraphy in Barnett Shale cores using energy-dispersive X-ray fluorescence (ED-XRF) and micro-rebound hammer hardness. Geological Society of America, Abstracts with Programs, v. 48, p. 241-248.

Wedepohl, K.H., 1971, Environmental influences on the chemical composition of shales and clays, in L.H. Ahrens, F. Press, S.K.Runcorn, and H.C. Urey, eds., Physics and Chemistry of the Earth, v. 8, p. 305-333.